JOURNAL OF GUIDANCE, CONTROL, AND DYNAMICS
Vol. 30, No. 3, May–June 2007

A Flight Simulation Algorithm for a Parafoil Suspending an Air Vehicle

Christiaan Redelinghuys*
University of Cape Town, Cape Town 7701, South Africa

DOI: 10.2514/1.25074

A mathematical model for the simulation of the motion of a parafoil suspending an unmanned air vehicle is developed. It is assumed that the parafoil and the air vehicle are rigid and that the suspension lines do not stretch. The configuration is allowed 8 degrees of freedom: six for the air vehicle and two relative rotations for the parafoil. A quasi-Hamiltonian formulation of the equations of motion is developed. The actual equation structure resembles the classic Hamiltonian form closely, avoiding the tedious differentiations of the generalized momenta with respect to time normally found in the Lagrangian approach. A structure for the calculation of parafoil aerodynamic parameters using data from computational fluid dynamics is proposed. Numerical stabilization of the constraint is discussed, and the results generated with the current method are compared to motion in vacuum, linearized trim flight solutions, and results generated by an existing parafoil modeling code. For the simulation of parafoil flight, the current quasi-Hamiltonian approach is reasonably straightforward to program using a tool such as MATLAB, avoiding the need to purchase expensive commercial multibody dynamics software.

Nomenclature

b_L	=	wing span of UAV
b_p	=	projected wing span of parafoil
C_D, C_L, C_Y	=	drag/lift/side force coefficients (in wind axes)
C_ℓ, C_m, C_n	=	rolling/pitching/yawing moment coefficients (for parafoil, in aerodynamic axes; for UAV, in body axes)
c_L, c_p	=	UAV/parafoil wing chords
E	=	energy
$\hat{\boldsymbol{e}}, \hat{\boldsymbol{i}}, \hat{\boldsymbol{j}}, \hat{\boldsymbol{k}}$	=	unit vectors
$\boldsymbol{F}$	=	force vector
f_{fudge}	=	adjustment factor to allow for parafoil distortion due to relative yaw
g	=	gravitational acceleration
H	=	Hamiltonian function or a matrix
$\boldsymbol{h}$	=	angular momentum vector
h_B, h_p	=	height of parafoil buoyancy/mass center above UAV mass center
I	=	moment or product of inertia (in case of parafoil, includes inertias of canopy, trapped air volume, and suspension lines)
$[I]$	=	unity matrix
$\bar{\boldsymbol{J}}$	=	Jacobian matrix
L	=	Lagrangian function
$\boldsymbol{M}$	=	moment
M_{rest}	=	internal suspension line restoring moment per unit line force
m_L	=	UAV mass
m_p	=	mass of parafoil (includes masses of canopy, trapped air volume, and suspension lines)
m_t	=	total mass of system
n	=	number of degrees of freedom
$\bar{\boldsymbol{P}}$	=	matrix
$\boldsymbol{p}$	=	generalized momentum vector
p, q, r	=	angular velocity components in body fixed axes
$\bar{p}, \bar{q}, \bar{r}$	=	dimensionless angular velocity components
$\boldsymbol{q}$	=	$\{X_L \quad Y_L \quad Z_L \quad \psi \quad \theta \quad \phi \quad \theta_r \quad \psi_r \quad z_c\}^T$
R	=	virtual distance from z_c axis to intersection of restoring force on canopy
$\bar{\boldsymbol{R}}$	=	matrix
$\boldsymbol{R}_9$	=	ninth row of matrix $\bar{\boldsymbol{R}}$
$\boldsymbol{r}$	=	position vector
r	=	lateral distance from UAV symmetry plane to hinge coupling
S_L	=	UAV wing area
S_p	=	parafoil projected wing area
$[T]$	=	transformation matrix
$\boldsymbol{V}$	=	velocity
V	=	speed, air volume, or components of a matrix
$[V_{\text{big}}]$	=	matrix
X_L, Y_L, Z_L	=	coordinates of UAV mass center in inertial axes
z_c	=	dummy coordinate at hinge
α, β	=	angle of attack/side-slip angle, or stability factors for $z_c = 0$ constraint
θ_A	=	rotation angle from parafoil aerodynamic to parafoil body axes
θ_r, ψ_r	=	parafoil pitch angle and yaw angle relative to UAV
λ	=	Lagrange multiplier = suspension line force
ρ	=	air density
σ	=	angle between suspension line force and z_c axis
$\boldsymbol{\Phi}$	=	$\{\psi \quad \theta \quad \phi\}^T$
$\boldsymbol{\Phi}_r$	=	$\{\theta_r \quad \psi_r\}^T$
ψ, θ, φ	=	UAV yaw, pitch, and roll Euler angles
Ω	=	matrix
$\boldsymbol{\omega}$	=	angular velocity

Subscripts

A	=	at point A or aerodynamic
H	=	hinge
I	=	inertial axes
L, p	=	UAV/parafoil
T	=	due to UAV thrust
w	=	wind axes or relative to wind

Received 16 June 2006; revision received 3 October 2006; accepted for publication 3 October 2006.

*Professor, Department of Mechanical Engineering. Member AIAA.

Introduction

RECOVERING unmanned air vehicles (UAVs) by means of guided parafoils, if made to work, is an attractive concept because it negates the necessity to land on a runway and improves the

mobility of the system [1]. To conceive the guidance and control algorithms for such a system, a model that can simulate the flight of the parafoil and UAV combination realistically is needed. A number of dynamic models for these configurations have seen the light. Lingard [2] summarized much of the early work and a recent publication by Yakimenko [3] contains a discussion of recent developments. Many of the previously developed models rely on classical Newtonian formulations in which both the parafoil and the UAV are treated as being rigid with 6 degrees of freedom each. At least three constraints are enforced at the suspension line coupling position, resulting in a system with 9 degrees of freedom, or less.

In the present study an 8 degrees of freedom model of the parafoil and UAV combination is developed by applying analytical mechanics. An advantage associated with analytical mechanics formulations (of which the well-known Lagrange method is one) is the fact that no constraint equations are needed if the number of generalized coordinates chosen equals the number of degrees of freedom. In the Lagrange equation approach, n second-order differential equations are generated for n independent generalized coordinates. Pillasch and Shen [4] developed Lagrange equations for a payload connected to a parachute by means of a friction and spreader plate mechanism. The physical nature of their parachute, connector, and payload differs vastly from that of a ram-air parafoil suspending a UAV, rendering their dynamic model inappropriate for the current investigation. The present approach resembles the classical Hamiltonian procedure in which n generalized momenta are introduced as auxiliary coordinates, leading to $2n$ first-order differential equations governing the motion. As will be discussed later, following the Hamiltonian approach avoids the tedious differentiation with respect to time required by the Lagrange method.

The current method relies on several assumptions. It is assumed that the configuration can be approximated by considering the parafoil canopy and the UAV to be rigid and the suspension lines and straps not to stretch. From observation of fight test maneuvers, considerable relative yaw and pitch, but little relative roll, occur between the parafoil and UAV. Hence only two coordinates describing relative motion between the parafoil and UAV were introduced: relative pitch and relative yaw. As trajectories considered are fairly short, a flat nonrotating earth was assumed. Although the dynamic formulation assumes a rigid parafoil canopy, the influence of parafoil warping on aerodynamic loads when asymmetric brakes are applied, is included. The aerodynamic model used here accommodates dynamic pressure, angle of attack and side-slip angle, relative yaw, brake application, and angular rates. Wind gusts may also occur.

The mathematical model discussed here was implemented in MATLAB. Any multidegree of freedom dynamics formulation is quite complex, necessitating quality assurance of the software. Various tests performed to confirm the validity of the code are reported later and it is shown that recently published solutions from linearized theory may be used to assess the validity of complex motion algorithms.

Kinematics of the Motion

Axes Systems and Generalized Coordinates

Figure 1 shows the various axes systems used. Definitions of the axes systems are summarized in Table 1 and the associated transformation matrices are presented in Appendix A.

Nine independent generalized coordinates are employed of which three, X_L, Y_L, and Z_L, fix the position of the UAV mass center in inertial axes. Three Euler angles describe the orientation of the UAV body axes with respect to inertial axes in the sequence ψ, θ, and φ (the rotations about the z_i axis, the intermediate y axis, and the x_L axis, respectively). The orientation of the parafoil relative to the UAV is defined by two rotations at the hinge: θ_r about the y_H axis followed by ψ_r about the z_p axis. A ninth coordinate, z_c, an imagined displacement of the hinge, is added to determine internal line force. This of course necessitates an equation of constraint $z_c = 0$ to be satisfied at all times.

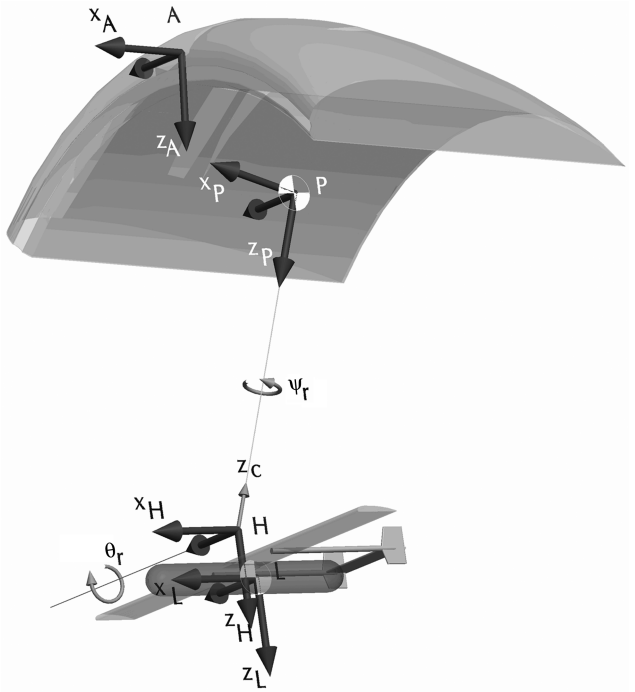

Fig. 1 Coordinates θ_r, ψ_r, and z_c and UAV body, hinge, parafoil body, and parafoil aerodynamic axes systems.

Velocities and Angular Velocities

The angular velocity of the UAV is given by

$$\boldsymbol{\omega}_L^L = \{\, p_L \quad q_L \quad r_L \,\}^T$$

Using the standard ψ, θ, φ sequence for Euler angles as described above, the UAV angular velocity components are related to the Euler angle rates via the equations [5]:

$$\begin{gathered} p_L = \dot{\phi} - \dot{\psi}\sin\theta \qquad q_L = \dot{\theta}\cos\phi + \dot{\psi}\cos\theta\sin\phi \\ r_L = \dot{\psi}\cos\theta\cos\phi - \dot{\theta}\sin\phi \end{gathered} \tag{1}$$

The angular velocity of the parafoil is given by

Table 1 Axes systems used

Name	Definition
Inertial axes	Origin at sea level x_i pointing north y_i pointing east z_i pointing down
UAV body axes	Origin at UAV mass center x_L pointing toward nose y_L pointing along UAV starboard wing z_L pointing down
Hinge axes	Origin midway between two suspension line coupling points (this origin is referred to as the "hinge") x_H, y_H, and z_H parallel to x_L, y_L, and z_L
Parafoil body axes	Origin at parafoil mass center x_p completes right-handed system y_p directed down the parafoil starboard wing z_p directed to the point midway between the two coupling points
Parafoil aerodynamic axes	Origin at parafoil nose in symmetry plane x_A pointing forward parallel to parafoil chord y_A pointing to right parallel to y_p z_A completes right-handed system
Parafoil wind axes	Origin at parafoil nose in symmetry plane x_w pointing into relative wind y_w to the right in x_w–y_A plane z_w completes right-handed system

$$\boldsymbol{\omega}_p = \boldsymbol{\omega}_L + \boldsymbol{\omega}_{p/L} \tag{2}$$

$$\boldsymbol{\omega}_{p/L} = \dot{\theta}_r \hat{\boldsymbol{j}}_L + \dot{\psi}_r \hat{\boldsymbol{k}}_p \tag{3}$$

Taking components in parafoil body axes, Eq. (2) becomes

$$\boldsymbol{\omega}_p^p = [T]_{pL} \boldsymbol{\omega}_L^L + [T]_{pL} \{0 \quad \dot{\theta}_r \quad 0\}^T + \{0 \quad 0 \quad \dot{\psi}_r\}^T \tag{4}$$

We seek a relationship between the parafoil mass center velocity, expressed in inertial axes, and the derivatives of the generalized coordinates. The velocity of the hinge relative to the UAV in UAV body axes is given by

$$\boldsymbol{V}_{H/L}^L = \boldsymbol{\omega}_L^L \times \boldsymbol{r}_{LH}^L = \{q_L z_{LH} \ (r_L x_{LH} - p_L z_{LH}) \ - q_L x_{LH}\}^T \tag{5}$$

Expanding and rearranging the relationship $\boldsymbol{V}_{H/L}^I = [T]_{LI}^T \boldsymbol{V}_{H/L}^L$, we have, in inertial axes,

$$\boldsymbol{V}_{H/L}^I = [V_{H/L}^I] \{\dot{\psi} \quad \dot{\theta} \quad \dot{\phi}\}^T \tag{6}$$

where the components of the 3×3 matrix $[V_{H/L}^I]$, listed in Appendix B, are functions of x_{LH}, z_{LH} and the coordinates ψ, θ, and φ. The velocity of the hinge in UAV body axes is

$$\boldsymbol{V}_H^L = [T]_{LI} \{\dot{X}_L \quad \dot{Y}_L \quad \dot{Z}_L\}^T + \boldsymbol{V}_{H/L}^L \tag{7}$$

The velocity of the parafoil mass center relative to the hinge in UAV body axes is

$$\boldsymbol{V}_{p/H}^L = -\dot{z}_c \hat{\boldsymbol{k}}_p^L + \boldsymbol{\omega}_p^L \times \boldsymbol{r}_{Hp}^L$$

Expanding and rearranging

$$\boldsymbol{V}_{p/H}^L = \left[V_{p/H}^p\right] \left\{\dot{\psi} \quad \dot{\theta} \quad \dot{\phi} \quad \dot{\theta}_r \quad \dot{\psi}_r \quad \dot{z}_c\right\}^T \tag{8}$$

where the components of the 3×6 matrix $[V_{p/H}^p]$, listed in Appendix B, are functions of z_{pH} and the coordinates ψ, θ, φ, and θ_r. With $[V_{p/H}^I] = [T]_{LI}^T [V_{p/H}^p]$, we finally obtain the velocity of the parafoil mass center taken in inertial axes as

$$\boldsymbol{V}_p^I = \begin{Bmatrix} \dot{X}_L \\ \dot{Y}_L \\ \dot{Z}_L \end{Bmatrix} + [V_{H/L}^I] \begin{Bmatrix} \dot{\psi} \\ \dot{\theta} \\ \dot{\phi} \end{Bmatrix} + [V_{p/H}^I] \begin{Bmatrix} \dot{\psi} \\ \dot{\theta} \\ \dot{\phi} \\ \dot{\theta}_r \\ \dot{\psi}_r \\ \dot{z}_c \end{Bmatrix} = [V_{\text{big}}] \{\dot{q}\} \tag{9}$$

$[V_{\text{big}}]$ is a 3×9 matrix, structured as follows:

$$\boldsymbol{V}_p^p = \boldsymbol{V}_H^p + \boldsymbol{V}_{p/H}^p = [T]_{pL} \boldsymbol{V}_H^L - \dot{z}_c \hat{\boldsymbol{k}}_p^p + \boldsymbol{\omega}_p^p \times \boldsymbol{r}_{Hp}^p = [T]_{pL} \boldsymbol{V}_H^L + \{-(z_{pH} + z_c) q_p \quad (z_{pH} + z_c) p_p \quad -\dot{z}_c\}^T \tag{11}$$

We need to determine aerodynamic loads, angles of attack, sideslip angles, and air speeds at the parafoil and UAV aerodynamic reference centers. The velocity of the parafoil aerodynamic reference center in parafoil axes is $\boldsymbol{V}_A^p = \boldsymbol{V}_p^p + \boldsymbol{\omega}_p^p \cdot \boldsymbol{r}_{pA}^p$. For the UAV and the parafoil the instantaneous velocity relative to the wind is, respectively, $\boldsymbol{V}_{Lw}^L = \boldsymbol{V}_L^L - \boldsymbol{V}_w^L$, and $\boldsymbol{V}_{Aw}^A = [T]_{pA}^T \{\boldsymbol{V}_A^p - \boldsymbol{V}_w^p\}$. The instantaneous aerodynamic angles are hence (provided that $\boldsymbol{V}_{L,Awx}^{L,A} \neq 0$ and $V_{L,Aw} \neq 0$): $\alpha_{L,A} = \tan^{-1}(\boldsymbol{V}_{L,Awx}^{L,A} / \boldsymbol{V}_{L,Awx}^{L,A})$ and $\beta_{L,A} = \sin^{-1}(\boldsymbol{V}_{L,Awy}^{L,A} / V_{L,Aw})$.

Lagrangian Function and Generalized Momenta

Considering both the parafoil and the UAV to be rigid bodies, the sum of translational and rotational energy for each is given by

$$E_{L,p\text{kin}} = \tfrac{1}{2} m_{L,p} V_{L,p}^2 + \tfrac{1}{2} \boldsymbol{\omega}_{L,p} \cdot \boldsymbol{h}_{L,p} \tag{12}$$

Two sources of potential energy will be considered, that due to weight and that due to buoyancy. The height difference between the parafoil and the UAV mass centers is given by

$$h_p = \{\boldsymbol{r}_{LH} - \boldsymbol{r}_{pH}\} \cdot (-\hat{\boldsymbol{k}}_I) = -T_{LI}(1,3)[x_{LH} - (z_{pH} + z_c) \sin\theta_r] - T_{LI}(3,3)[z_{LH} - (z_{pH} + z_c) \cos\theta_r] \tag{13}$$

Similarly, the height difference between the parafoil buoyancy center and the UAV mass center is

$$h_B = \{\boldsymbol{r}_{LH} - \boldsymbol{r}_{BH}\} \cdot (-\hat{\boldsymbol{k}}_I) = -T_{LI}(1,3)[x_{LH} - x_{BH} \cos\theta_r \cos\psi_r - (z_{BH} + z_c) \sin\theta_r] + T_{LI}(2,3) x_{BH} \sin\psi_r - T_{LI}(3,3)[z_{LH} + x_{BH} \sin\theta_r \cos\psi_r - (z_{BH} + z_c) \cos\theta_r] \tag{14}$$

The system potential energy thus becomes $E_{\text{pot}} = -m_t g Z_L + m_p g h_p - \rho V g (h_B - Z_L)$, allowing the Lagrangian for the configuration to be summarized as

$$L = E_{L\text{kin}} + E_{p\text{kin}} - E_{\text{pot}} = \tfrac{1}{2}\{m_L \boldsymbol{V}_L \cdot \boldsymbol{V}_L + m_p \boldsymbol{V}_p \cdot \boldsymbol{V}_p + \boldsymbol{\omega}_L \cdot \boldsymbol{h}_L + \boldsymbol{\omega}_p \cdot \boldsymbol{h}_p\} + m_t g Z_L - m_p g h_p + \rho V g (h_B - Z_L) \tag{15}$$

The derivatives of L with respect to the rates of change of the generalized coordinates produce the so-called generalized momenta. For the position coordinates X_L, Y_L, and Z_L we have

$$[V_{\text{big}}] = \begin{bmatrix} 1 & 0 & 0 & 0 & 0 & 0 & 0 & 0 & 0 \\ 0 & 1 & 0 & 0 & 0 & 0 & 0 & 0 & 0 \\ 0 & 0 & 1 & 0 & 0 & 0 & 0 & 0 & 0 \end{bmatrix} + \begin{bmatrix} 0 & 0 & 0 & V_{H/L}^I(1,1) & V_{H/L}^I(1,2) & V_{H/L}^I(1,3) & 0 & 0 & 0 \\ 0 & 0 & 0 & V_{H/L}^I(2,1) & V_{H/L}^I(2,2) & V_{H/L}^I(2,3) & 0 & 0 & 0 \\ 0 & 0 & 0 & V_{H/L}^I(3,1) & V_{H/L}^I(3,2) & V_{H/L}^I(3,3) & 0 & 0 & 0 \end{bmatrix} + \begin{bmatrix} 0 & 0 & 0 & V_{p/H}^I(1,1) & V_{p/H}^I(1,2) & V_{p/H}^I(1,3) & V_{p/H}^I(1,4) & V_{p/H}^I(1,5) & V_{p/H}^I(1,6) \\ 0 & 0 & 0 & V_{p/H}^I(2,1) & V_{p/H}^I(2,2) & V_{p/H}^I(2,3) & V_{p/H}^I(2,4) & V_{p/H}^I(2,5) & V_{p/H}^I(2,6) \\ 0 & 0 & 0 & V_{p/H}^I(3,1) & V_{p/H}^I(3,2) & V_{p/H}^I(3,3) & V_{p/H}^I(3,4) & V_{p/H}^I(3,5) & V_{p/H}^I(3,6) \end{bmatrix} \tag{10}$$

Equation (9) is the desired relationship between parafoil velocity and the derivatives of the coordinates to be used in the dynamic analysis below. It will be useful to also express the parafoil mass center velocity in parafoil axes, as follows:

$$\boldsymbol{p}_{\text{lin}} \equiv \{p_{XI} \quad p_{YI} \quad p_{ZI}\}^T = \frac{\partial L}{\partial \dot{\boldsymbol{r}}_L} \equiv \left\{\frac{\partial L}{\partial \dot{X}_L} \quad \frac{\partial L}{\partial \dot{Y}_L} \quad \frac{\partial L}{\partial \dot{Z}_L}\right\}^T$$

Now, from Eqs. (9), (10), and (15),

$$\frac{\partial L}{\partial \dot{\boldsymbol{r}}_L} = m_L \boldsymbol{V}_L^I + m_p \boldsymbol{V}_p^I$$
$$= \left\{ m_L \begin{bmatrix} 1 & 0 & 0 & 0 & 0 & 0 & 0 & 0 & 0 \\ 0 & 1 & 0 & 0 & 0 & 0 & 0 & 0 & 0 \\ 0 & 0 & 1 & 0 & 0 & 0 & 0 & 0 & 0 \end{bmatrix} + m_p [V_{\text{big}}] \right\} \{\dot{q}\}$$

For the UAV rotational coordinates ψ, θ, and φ, we have

$$\boldsymbol{p}_{\text{rot1}} \equiv \{ p_\psi \quad p_\theta \quad p_\phi \}^T = \frac{\partial L}{\partial \dot{\boldsymbol{\Phi}}} \equiv \left\{ \frac{\partial L}{\partial \dot{\psi}} \quad \frac{\partial L}{\partial \dot{\theta}} \quad \frac{\partial L}{\partial \dot{\phi}} \right\}^T$$

We choose body axes systems for the expansion of the rotational terms of Eq. (15) with respect to ψ, θ, and φ. This implies that the inertia tensors are time invariant. Exploiting the fact that the inertia tensors are symmetric, it can easily be shown using Eq. (15) that

$$\frac{\partial L}{\partial \dot{\boldsymbol{\Phi}}} = \frac{\partial \boldsymbol{\omega}_L^L}{\partial \dot{\boldsymbol{\Phi}}} \boldsymbol{h}_L^L + \frac{\partial \boldsymbol{\omega}_p^p}{\partial \dot{\boldsymbol{\Phi}}} \boldsymbol{h}_p^p + m_p \frac{\partial \boldsymbol{V}_p^I}{\partial \dot{\boldsymbol{\Phi}}} \boldsymbol{V}_p^I \tag{16}$$

where the partial derivatives on the right-hand side are 3×3 matrices. We allow a single product of inertia in the longitudinal plane for both the UAV and the parafoil. For each body, the angular momentum is expressed in term of the generalized coordinates, as follows:

$$\boldsymbol{h}_{L,p}^{L,p} = \begin{bmatrix} I_{L,pxx} & 0 & I_{L,pxz} \\ 0 & I_{L,pyy} & 0 \\ I_{L,pxz} & 0 & I_{L,pzz} \end{bmatrix} \begin{Bmatrix} p_{L,p} \\ q_{L,p} \\ r_{L,p} \end{Bmatrix}$$
$$= \begin{Bmatrix} I_{L,pxx} p_{L,p} + I_{L,pxz} r_{L,p} \\ I_{L,pyy} q_{L,p} \\ I_{L,pxz} p_{L,p} + I_{L,pzz} r_{L,p} \end{Bmatrix} \tag{17}$$

Using Eqs. (1) and (4), Eq. (17) can be rearranged to give

$$\boldsymbol{h}_L^L = [H_L] \{ \dot{\psi} \quad \dot{\theta} \quad \dot{\phi} \}^T \tag{18}$$

and

$$\boldsymbol{h}_p^p = [H_p] \{ \dot{\psi} \quad \dot{\theta} \quad \dot{\phi} \quad \dot{\theta}_r \quad \dot{\psi}_r \}^T \tag{19}$$

where $[H_L]$ and $[H_p]$ are a 3×3 and a 3×5 matrix, respectively, with components, expanded in Appendix B, depending on the angular generalized coordinates. The partial derivatives contained in Eq. (16) are now expanded.

$$\frac{\partial \boldsymbol{\omega}_{L,p}^{L,p}}{\partial \dot{\boldsymbol{\Phi}}} = \begin{bmatrix} \frac{\partial p_{L,p}}{\partial \dot{\psi}} & \frac{\partial q_{L,p}}{\partial \dot{\psi}} & \frac{\partial r_{L,p}}{\partial \dot{\psi}} \\ \frac{\partial p_{L,p}}{\partial \dot{\theta}} & \frac{\partial q_{L,p}}{\partial \dot{\theta}} & \frac{\partial r_{L,p}}{\partial \dot{\theta}} \\ \frac{\partial p_{L,p}}{\partial \dot{\phi}} & \frac{\partial q_{L,p}}{\partial \dot{\phi}} & \frac{\partial r_{L,p}}{\partial \dot{\phi}} \end{bmatrix} \equiv [\Omega_{L,p}] \tag{20}$$

Using Eq. (1), the components of the 3×3 matrix $[\Omega_L]$ can be obtained. The result is shown in Appendix B. From Eq. (4) it follows that $[\Omega_p] = [\Omega_L][T]_{pL}^T$. The matrix in the last term of Eq. (16) can easily be obtained by noting that the partial derivatives of parafoil velocity with respect to the derivatives of the generalized coordinates are simply the respective columns of the matrix $[V_{\text{big}}]$. Hence

$$\frac{\partial \boldsymbol{V}_p^I}{\partial \dot{\boldsymbol{\Phi}}} = \begin{bmatrix} \frac{\partial V_{px}^I}{\partial \dot{\psi}} & \frac{\partial V_{py}^I}{\partial \dot{\psi}} & \frac{\partial V_{pz}^I}{\partial \dot{\psi}} \\ \frac{\partial V_{px}^I}{\partial \dot{\theta}} & \frac{\partial V_{py}^I}{\partial \dot{\theta}} & \frac{\partial V_{pz}^I}{\partial \dot{\theta}} \\ \frac{\partial V_{px}^I}{\partial \dot{\phi}} & \frac{\partial V_{py}^I}{\partial \dot{\phi}} & \frac{\partial V_{pz}^I}{\partial \dot{\phi}} \end{bmatrix}$$
$$= \begin{bmatrix} V_{\text{big}}(1,4) & V_{\text{big}}(2,4) & V_{\text{big}}(3,4) \\ V_{\text{big}}(1,5) & V_{\text{big}}(2,5) & V_{\text{big}}(3,5) \\ V_{\text{big}}(1,6) & V_{\text{big}}(2,6) & V_{\text{big}}(3,6) \end{bmatrix} \equiv [V_{\text{big1}}]$$

Similarly, the generalized momenta for the parafoil relative rotations, θ_r and ψ_r, are

$$\boldsymbol{p}_{\text{rotr}} \equiv \{ p_{\theta r} \quad p_{\psi r} \}^T = \frac{\partial L}{\partial \dot{\boldsymbol{\Phi}}_r} \equiv \left\{ \frac{\partial L}{\partial \dot{\theta}_r} \quad \frac{\partial L}{\partial \dot{\psi}_r} \right\}^T$$

The energy of the UAV is of course not influenced by the relative rotations. Thus, using Eq. (15),

$$\frac{\partial L}{\partial \dot{\boldsymbol{\Phi}}_r} = \frac{\partial \boldsymbol{\omega}_p^p}{\partial \dot{\boldsymbol{\Phi}}_r} \boldsymbol{h}_p^p + m_p \frac{\partial \boldsymbol{V}_p^I}{\partial \dot{\boldsymbol{\Phi}}_r} \boldsymbol{V}_p^I \tag{21}$$

The partial derivatives on the right-hand side of Eq. (21) now represent 2×3 matrices.

$$\frac{\partial \boldsymbol{\omega}_p^p}{\partial \dot{\boldsymbol{\Phi}}_r} = \begin{bmatrix} \frac{\partial p_p}{\partial \dot{\theta}_r} & \frac{\partial q_p}{\partial \dot{\theta}_r} & \frac{\partial r_p}{\partial \dot{\theta}_r} \\ \frac{\partial p_p}{\partial \dot{\psi}_r} & \frac{\partial q_p}{\partial \dot{\psi}_r} & \frac{\partial r_p}{\partial \dot{\psi}_r} \end{bmatrix} \equiv [\Omega_{pr}] \tag{22}$$

Using Eqs. (1) and (4), the components of the 3×3 matrix $[\Omega_{pr}]$ can be obtained. The result is shown in Appendix B. Using the columns of $[V_{\text{big}}]$:

$$\frac{\partial \boldsymbol{V}_p^I}{\partial \dot{\boldsymbol{\Phi}}_r} = \begin{bmatrix} \frac{\partial V_{px}^I}{\partial \dot{\theta}_r} & \frac{\partial V_{py}^I}{\partial \dot{\theta}_r} & \frac{\partial V_{pz}^I}{\partial \dot{\theta}_r} \\ \frac{\partial V_{px}^I}{\partial \dot{\psi}_r} & \frac{\partial V_{py}^I}{\partial \dot{\psi}_r} & \frac{\partial V_{pz}^I}{\partial \dot{\psi}_r} \end{bmatrix}$$
$$= \begin{bmatrix} V_{\text{big}}(1,7) & V_{\text{big}}(2,7) & V_{\text{big}}(3,7) \\ V_{\text{big}}(1,8) & V_{\text{big}}(2,8) & V_{\text{big}}(3,8) \end{bmatrix} \equiv [V_{\text{big2}}]$$

For the coordinate z_c, we have, from Eqs. (11) and (15),

$$\boldsymbol{p}_{zc} = \frac{\partial L}{\partial \dot{z}_c} = m_p \frac{\partial \boldsymbol{V}_p^p}{\partial \dot{z}_c} \cdot \boldsymbol{V}_p^p = -m_p V_z^p$$

or

$$\boldsymbol{p}_{zc} = m_p \frac{\partial \boldsymbol{V}_p^I}{\partial \dot{z}_c} \cdot \boldsymbol{V}_p^I$$
$$= m_p \{ V_{\text{big}}(1,9) \quad V_{\text{big}}(2,9) \quad V_{\text{big}}(3,9) \} [V_{\text{big}}] \{\dot{q}\}$$

The vector $\boldsymbol{p}_{\text{lin}}$ represents the linear momentum of the system. The components of the vector $\boldsymbol{p}_{\text{rot1}}$ are system angular momenta with respect to a point instantaneously corresponding to the UAV mass center, directed along the rotation axes for ψ, θ, and φ. Similarly, the components of $\boldsymbol{p}_{\text{rotr}}$ are parafoil angular momenta with respect to a point instantaneously corresponding to the hinge point, directed along the rotation axes θ_r and ψ_r. Finally, the linear momentum of the parafoil, directed from the hinge to the parafoil mass center, is associated with $\boldsymbol{p}_{zc}$.

In the Lagrange approach time derivatives of the various generalized momenta are computed to develop the equations of motion. In the present approach this tedious step is avoided by following a Hamiltonian approach. As a first step in developing a Hamiltonian formulation a relationship between the generalized momenta and the generalized velocities is sought. This can be achieved by consolidation of the kinematic equations as developed above. The result is

$$\boldsymbol{p} = \bar{\boldsymbol{P}} \dot{\boldsymbol{q}} \tag{23}$$

where $\boldsymbol{p} = \{ p_{XI} \; p_{YI} \; p_{ZI} \; p_\psi \; p_\vartheta \; p_\phi \; p_{\theta r} \; p_{\psi r} \; p_{zc} \}^T$ and $\bar{\boldsymbol{P}}$ is a 9×9 matrix depending on the generalized coordinates and geometric parameters. This matrix is divided into submatrices, each defined as indicated below:

$$\bar{\boldsymbol{P}}_1 \equiv m_p [V_{\text{big1}}] + m_L \begin{bmatrix} 1 & 0 & 0 & 0 & 0 & 0 & 0 & 0 & 0 \\ 0 & 1 & 0 & 0 & 0 & 0 & 0 & 0 & 0 \\ 0 & 0 & 1 & 0 & 0 & 0 & 0 & 0 & 0 \end{bmatrix}$$

With $\bar{\boldsymbol{P}}_{2a} \equiv [\Omega_L][H_L]$, $\bar{\boldsymbol{P}}_{2b} \equiv [\Omega_p][H_p]$, and $\bar{\boldsymbol{P}}_{2c} \equiv [V_{\text{big1}}][V_{\text{big}}]$,

$$\bar{\boldsymbol{P}}_2 \equiv \begin{bmatrix} 0 & 0 & 0 & P_{2a}(1,1) & P_{2a}(1,2) & P_{2a}(1,3) & 0 & 0 & 0 \\ 0 & 0 & 0 & P_{2a}(2,1) & P_{2a}(2,2) & P_{2a}(2,3) & 0 & 0 & 0 \\ 0 & 0 & 0 & P_{2a}(3,1) & P_{2a}(3,2) & P_{2a}(3,3) & 0 & 0 & 0 \end{bmatrix} + \begin{bmatrix} 0 & 0 & 0 & P_{2b}(1,1) & P_{2b}(1,2) & P_{2b}(1,3) & P_{2b}(1,4) & P_{2b}(1,5) & 0 \\ 0 & 0 & 0 & P_{2b}(2,1) & P_{2b}(2,2) & P_{2b}(2,3) & P_{2b}(2,4) & P_{2b}(2,5) & 0 \\ 0 & 0 & 0 & P_{2b}(3,1) & P_{2b}(3,2) & P_{2b}(3,3) & P_{2b}(3,4) & P_{2b}(3,5) & 0 \end{bmatrix} + m_p \bar{\boldsymbol{P}}_{2c}$$

With $\bar{\boldsymbol{P}}_{3a} \equiv [\Omega_{pr}][H_p]$ and $\bar{\boldsymbol{P}}_{3b} \equiv [V_{\text{big2}}][V_{\text{big}}]$,

$$\bar{\boldsymbol{P}}_3 \equiv \begin{bmatrix} 0 & 0 & 0 & P_{3a}(1,1) & P_{3a}(1,2) & P_{3a}(1,3) & P_{3a}(1,4) & P_{3a}(1,5) & 0 \\ 0 & 0 & 0 & P_{3a}(2,1) & P_{3a}(2,2) & P_{3a}(2,3) & P_{3a}(2,4) & P_{3a}(2,5) & 0 \end{bmatrix} + m_p \bar{\boldsymbol{P}}_{3b} \quad \text{and}$$

$$\bar{\boldsymbol{P}}_4 \equiv m_p \{ \, V_{\text{big}}(1,9) \quad V_{\text{big}}(2,9) \quad V_{\text{big}}(3,9) \, \} [V_{\text{big}}]$$

Finally, we have

$$\bar{\boldsymbol{P}} = \begin{bmatrix} \bar{\boldsymbol{P}}_1 \\ \bar{\boldsymbol{P}}_2 \\ \bar{\boldsymbol{P}}_3 \\ \bar{\boldsymbol{P}}_4 \end{bmatrix}$$

Dynamics

The Hamiltonian formulation of the equations of motion [6] is obtained by forming the Hamiltonian $H = \boldsymbol{p} \cdot \dot{\boldsymbol{q}} - L$. The Hamiltonian canonical form is

$$\dot{\boldsymbol{q}} = \frac{\partial H}{\partial \boldsymbol{p}}, \qquad \dot{\boldsymbol{p}} = -\frac{\partial H}{\partial \boldsymbol{q}} + \boldsymbol{\lambda} + \boldsymbol{Q} \tag{24}$$

where $\boldsymbol{\lambda} = \{0\ 0\ 0\ 0\ 0\ 0\ 0\ 0\ -\lambda\}^T$ as we have one constraint equation, $z_c = 0$. In the present development this approach is adapted by using Eq. (23) instead of the first of Eq. (24). In other words, the $2n$ first-order differential equations to be solved here are

$$\dot{\boldsymbol{q}} = \bar{\boldsymbol{P}}^{-1} \boldsymbol{p} \tag{25}$$

and

$$\dot{\boldsymbol{p}} = \frac{\partial L}{\partial \boldsymbol{q}} + \boldsymbol{\lambda} + \boldsymbol{Q} \tag{26}$$

Equation (26) is of course the standard set of Lagrange equations. To complete the formulation we have to obtain expressions for the right-hand side of Eq. (26).

Derivatives of the Lagrangian with Respect to the Generalized Coordinates

For the position coordinates it can easily be shown that

$$\frac{\partial L}{\partial \boldsymbol{r}} = \{ 0 \quad 0 \quad m_t g \}^T - \{ 0 \quad 0 \quad \rho V g \}^T \tag{27}$$

For the rotational coordinates ψ, θ, and φ, it follows from Eq. (15) that

$$\frac{\partial L}{\partial \boldsymbol{\Phi}} = \frac{\partial \boldsymbol{\omega}_L^L}{\partial \boldsymbol{\Phi}} \boldsymbol{h}_L^L + \frac{\partial \boldsymbol{\omega}_p^p}{\partial \boldsymbol{\Phi}} \boldsymbol{h}_p^p + m_p \frac{\partial \boldsymbol{V}_p^p}{\partial \boldsymbol{\Phi}} \boldsymbol{V}_p^p - m_p g \frac{\partial h_p}{\partial \boldsymbol{\Phi}} + \rho V g \frac{\partial h_B}{\partial \boldsymbol{\Phi}} \tag{28}$$

The 3×3 matrices on the right-hand side of Eq. (28) are found, just as before,

$$\frac{\partial \boldsymbol{\omega}_{L,p}^{L,p}}{\partial \boldsymbol{\Phi}} = \begin{bmatrix} \frac{\partial p_{L,p}}{\partial \psi} & \frac{\partial q_{L,p}}{\partial \psi} & \frac{\partial r_{L,p}}{\partial \psi} \\ \frac{\partial p_{L,p}}{\partial \theta} & \frac{\partial q_{L,p}}{\partial \theta} & \frac{\partial r_{L,p}}{\partial \theta} \\ \frac{\partial p_{L,p}}{\partial \phi} & \frac{\partial q_{L,p}}{\partial \phi} & \frac{\partial r_{L,p}}{\partial \phi} \end{bmatrix} \equiv [\Omega_{\Phi L,p}] \tag{29}$$

Using Eq. (1), the components of the 3×3 matrices $[\Omega_{\Phi L}]$ can be obtained. The result is shown in Appendix B. From Eq. (4) it follows that $[\Omega_{\Phi p}] = [\Omega_{\Phi L}][T]_{pL}^T$.

The matrix in the third term on the right-hand side of Eq. (28) can be obtained by noting that

$$\frac{\partial \boldsymbol{V}_p^p}{\partial \boldsymbol{\Phi}} = \begin{bmatrix} \frac{\partial V_{px}^p}{\partial \psi} & \frac{\partial V_{py}^p}{\partial \psi} & \frac{\partial V_{pz}^p}{\partial \psi} \\ \frac{\partial V_{px}^p}{\partial \theta} & \frac{\partial V_{py}^p}{\partial \theta} & \frac{\partial V_{pz}^p}{\partial \theta} \\ \frac{\partial V_{px}^p}{\partial \phi} & \frac{\partial V_{py}^p}{\partial \phi} & \frac{\partial V_{pz}^p}{\partial \phi} \end{bmatrix} \equiv [V_{\Phi p}] \tag{30}$$

Taking the transpose of Eq. (11) and differentiating,

$$[V_{\Phi p}] = \frac{\partial \boldsymbol{V}_H^L}{\partial \boldsymbol{\Phi}}[T]_{pL}^T + \frac{\partial \boldsymbol{V}_{p/H}^p}{\partial \boldsymbol{\Phi}} \tag{31}$$

and, using Eq. (7):

$$\frac{\partial \boldsymbol{V}_H^L}{\partial \boldsymbol{\Phi}} = \left[\{ \dot{X}_L \quad \dot{Y}_L \quad \dot{Z}_L \} \begin{pmatrix} [T_\psi]_{LI}^T \\ [T_\theta]_{LI}^T \\ [T_\phi]_{LI}^T \end{pmatrix} \right] + [V_{\Phi H/L}] \tag{32}$$

where the partial derivatives of the transformation matrices are shown in Appendix B and, using Eq. (5):

$$\begin{aligned} [V_{\Phi H/L}] \equiv \frac{\partial}{\partial \boldsymbol{\Phi}}(\boldsymbol{\omega}_L^L \times \boldsymbol{r}_{LH}^L) &= \frac{\partial}{\partial \boldsymbol{\Phi}} \{ q_L z_{LH} \quad (r_L x_{LH} - p_L z_{LH}) \quad -q_L x_{LH} \}^T \\ &= \begin{bmatrix} z_{LH}\Omega_{\Phi L}(1,2) & x_{LH}\Omega_{\Phi L}(1,3) - z_{LH}\Omega_{\Phi L}(1,1) & -x_{LH}\Omega_{\Phi L}(1,2) \\ z_{LH}\Omega_{\Phi L}(2,2) & x_{LH}\Omega_{\Phi L}(2,3) - z_{LH}\Omega_{\Phi L}(2,1) & -x_{LH}\Omega_{\Phi L}(2,2) \\ z_{LH}\Omega_{\Phi L}(3,2) & x_{LH}\Omega_{\Phi L}(3,3) - z_{LH}\Omega_{\Phi L}(3,1) & -x_{LH}\Omega_{\Phi L}(3,2) \end{bmatrix} \end{aligned} \tag{33}$$

It follows from the last of Eq. (11) that

$$\frac{\partial \boldsymbol{V}_{p/H}^p}{\partial \boldsymbol{\Phi}} = \begin{bmatrix} -(z_{pH}+z_c)\Omega_{\Phi p}(1,2) & (z_{pH}+z_c)\Omega_{\Phi p}(1,1) & 0 \\ -(z_{pH}+z_c)\Omega_{\Phi p}(2,2) & (z_{pH}+z_c)\Omega_{\Phi p}(2,1) & 0 \\ -(z_{pH}+z_c)\Omega_{\Phi p}(3,2) & (z_{pH}+z_c)\Omega_{\Phi p}(3,1) & 0 \end{bmatrix} \tag{34}$$

Equation (31) thus becomes

$$[V_{\Phi p}] = \left\{ \left[\{ \dot{X}_L \quad \dot{Y}_L \quad \dot{Z}_L \} \begin{pmatrix} [T_\psi]_{LI}^T \\ [T_\theta]_{LI}^T \\ [T_\phi]_{LI}^T \end{pmatrix} \right] + [V_{\Phi H/L}] \right\} [T]_{pL}^T + \begin{bmatrix} -(z_{pH}+z_c)\Omega_{\Phi p}(1,2) & (z_{pH}+z_c)\Omega_{\Phi p}(1,1) & 0 \\ -(z_{pH}+z_c)\Omega_{\Phi p}(2,2) & (z_{pH}+z_c)\Omega_{\Phi p}(2,1) & 0 \\ -(z_{pH}+z_c)\Omega_{\Phi p}(3,2) & (z_{pH}+z_c)\Omega_{\Phi p}(3,1) & 0 \end{bmatrix} \tag{35}$$

The weight term in Eq. (28) is expanded, using Eqs. (13) and (A1).

$$\frac{\partial h_p}{\partial \boldsymbol{\Phi}} = \begin{Bmatrix} 0 \\ \cos\theta[x_{LH} - (z_{pH}+z_c)\sin\theta_r] + \sin\theta\cos\phi[z_{LH} - (z_{pH}+z_c)\cos\theta_r] \\ \cos\theta\sin\phi[z_{LH} - (z_{pH}+z_c)\cos\theta_r] \end{Bmatrix} \tag{36}$$

and the buoyancy term follows from differentiating Eq. (14):

$$\frac{\partial h_B}{\partial \boldsymbol{\Phi}} = \begin{Bmatrix} 0 \\ -T_{LI\theta}(1,3)\ell_1 + T_{LI\theta}(2,3)\ell_2 - T_{LI\theta}(3,3)\ell_3 \\ -T_{LI\phi}(1,3)\ell_1 + T_{LI\phi}(2,3)\ell_2 - T_{LI\phi}(3,3)\ell_3 \end{Bmatrix} \tag{37}$$

where

$$\ell_1 \equiv x_{LH} - x_{BH}\cos\theta_r\cos\psi_r - (z_{BH}+z_c)\sin\theta_r \qquad \ell_2 \equiv x_{BH}\sin\psi_r \qquad \ell_3 \equiv z_{LH} + x_{BH}\sin\theta_r\cos\psi_r - (z_{BH}+z_c)\cos\theta_r \tag{38}$$

The last two terms in Eq. (28) have a physical meaning. The first of these represents moments due to parafoil weight about the UAV mass center along the ψ, θ, and φ rotational axes. The other term represents moments due to the buoyancy force about the UAV mass center along the same axes. All the terms of Eq. (28) have now been developed.

A similar procedure will be followed for the two coordinates, θ_r and ψ_r. From Eq. (15)

$$\frac{\partial L}{\partial \boldsymbol{\Phi}_r} = \frac{\partial \boldsymbol{\omega}_p^p}{\partial \boldsymbol{\Phi}_r}\boldsymbol{h}_p^p + m_p \frac{\partial \boldsymbol{V}_p^p}{\partial \boldsymbol{\Phi}_r}\boldsymbol{V}_p^p - m_p g \frac{\partial h_p}{\partial \boldsymbol{\Phi}_r} + \rho V g \frac{\partial h_B}{\partial \boldsymbol{\Phi}_r} \tag{39}$$

where

$$\frac{\partial \boldsymbol{\omega}_p^p}{\partial \boldsymbol{\Phi}_r} = \begin{bmatrix} \frac{\partial p_p}{\partial \theta_r} & \frac{\partial q_p}{\partial \theta_r} & \frac{\partial r_p}{\partial \theta_r} \\ \frac{\partial p_p}{\partial \psi_r} & \frac{\partial q_p}{\partial \psi_r} & \frac{\partial r_p}{\partial \psi_r} \end{bmatrix} \equiv [\Omega_{\Phi rp}] \tag{40}$$

By suitably differentiating Eq. (4), we obtain

$$[\Omega_{\Phi rp}] = \{ p_L \quad q_L + \dot{\theta}_r \quad r_L \} \begin{pmatrix} [T_{\theta r}]_{pL}^T \\ [T_{\psi r}]_{pL}^T \end{pmatrix} \tag{41}$$

Expansions of the matrices $[T_{\theta r}]_{pL}$ and $[T_{\psi r}]_{pL}$ can be found in Appendix B.

$$\frac{\partial \boldsymbol{V}_p^p}{\partial \boldsymbol{\Phi}_r} = \begin{bmatrix} \frac{\partial V_{px}^p}{\partial \theta_r} & \frac{\partial V_{py}^p}{\partial \theta_r} & \frac{\partial V_{pz}^p}{\partial \theta_r} \\ \frac{\partial V_{px}^p}{\partial \psi_r} & \frac{\partial V_{py}^p}{\partial \psi_r} & \frac{\partial V_{pz}^p}{\partial \psi_r} \end{bmatrix} \equiv [V_{\Phi rp}] \tag{42}$$

Differentiating the transpose of Eq. (11):

$$[V_{\Phi rp}] = \boldsymbol{V}_H^{LT}\begin{pmatrix}[T_{\theta r}]_{pL}^T\\ [T_{\psi r}]_{pL}^T\end{pmatrix} + \frac{\partial \boldsymbol{V}_{p/H}^p}{\partial \boldsymbol{\Phi}_r} = \boldsymbol{V}_H^{LT}\begin{pmatrix}[T_{\theta r}]_{pL}^T\\ [T_{\psi r}]_{pL}^T\end{pmatrix} + \begin{bmatrix} -(z_{pH}+z_c)\Omega_{\Phi rp}(1,2) & (z_{pH}+z_c)\Omega_{\Phi rp}(1,1) & 0\\ -(z_{pH}+z_c)\Omega_{\Phi rp}(2,2) & (z_{pH}+z_c)\Omega_{\Phi rp}(2,1) & 0\end{bmatrix} \quad (43)$$

The weight term in Eq. (39) is found using Eq. (13):

$$\frac{\partial h_p}{\partial \boldsymbol{\Phi}_r} = \begin{Bmatrix}(z_{pH}+z_c)[T_{LI}(1,3)\cos\theta_r - T_{LI}(3,3)\sin\theta_r]\\ 0\end{Bmatrix}$$

and, similarly, for the buoyancy term, from Eq. (14):

$$\frac{\partial h_B}{\partial \boldsymbol{\Phi}_r} = \begin{Bmatrix}-T_{LI}(1,3)[x_{BH}\sin\theta_r\cos\psi_r - (z_{BH}+z_c)\cos\theta_r] - T_{LI}(3,3)[x_{BH}\cos\theta_r\cos\psi_r + (z_{BH}+z_c)\sin\theta_r]\\ -T_{LI}(1,3)x_{BH}\cos\theta_r\sin\psi_r + T_{LI}(2,3)x_{BH}\cos\psi_r + T_{LI}(3,3)x_{BH}\sin\theta_r\sin\psi_r\end{Bmatrix}$$

For the remaining coordinate, z_c, we have using Eq. (15):

$$\frac{\partial L}{\partial z_c} = m_p\frac{\partial \boldsymbol{V}_p^p}{\partial z_c}\cdot\boldsymbol{V}_p^p - m_p g\frac{\partial h_p}{\partial z_c} + \rho V g\frac{\partial h_B}{\partial z_c}$$

From Eq. (11) it follows that

$$\frac{\partial \boldsymbol{V}_p^p}{\partial z_c} = \{-q_p \quad p_p \quad 0\}^T$$

Hence

$$m_p\frac{\partial \boldsymbol{V}_p^p}{\partial z_c}\cdot\boldsymbol{V}_p^p = m_p(-q_pV_{px}^p + r_pV_{py}^p)$$

From Eqs. (13) and (14) it follows that

$$\frac{\partial h_p}{\partial z_c} = T_{LI}(3,3)\cos\theta_r + T_{LI}(1,3)\sin\theta_r = \frac{\partial h_B}{\partial z_c}$$

The last two terms in Eq. (39) have a physical meaning similar to their counterparts in Eq. (28). The first of these terms represents moments due to parafoil weight about the hinge along the θ_r and ψ_r rotational axes. The other term represents moments due to the buoyancy force about the hinge along the same axes. All the terms of Eq. (39) have now been expanded.

Equation of Constraint

As was mentioned before, a dummy coordinate, z_c, was added to the formulation to enable calculation of the instantaneous resultant of the suspension line force. The equation of constraint is of course just $z_c = 0$. However, this equation has to be developed to a form suitable for inclusion in the numerical integration procedure, duly considering numerical stability. First note that, if we define $\bar{\boldsymbol{R}} \equiv \bar{\boldsymbol{P}}^{-1}$, we obtain from Eq. (25) and application of the condition of constraint

$$\dot{z}_c = \boldsymbol{R}_9^T\cdot\boldsymbol{p} = 0 \quad (44)$$

Taking the time derivative of Eq. (44) leaves

$$\ddot{z}_c = \dot{\boldsymbol{R}}_9^T\cdot\boldsymbol{p} + \boldsymbol{R}_9^T\cdot\dot{\boldsymbol{p}} = 0 \quad (45)$$

The matrices $\bar{\boldsymbol{R}}$ and $\bar{\boldsymbol{P}}$ depend only on the system geometry and the generalized coordinates $\boldsymbol{q}$. Hence we can write

$$\dot{\boldsymbol{R}}_9 = \bar{\boldsymbol{J}}\,\dot{\boldsymbol{q}} \quad (46)$$

where

$$\bar{\boldsymbol{J}} \equiv \begin{bmatrix} R(9,1)_{q1} & R(9,1)_{q2} & \cdots & R(9,1)_{q9}\\ R(9,2)_{q1} & R(9,2)_{q2} & \cdots & R(9,2)_{q9}\\ \vdots & \vdots & \vdots & \vdots\\ R(9,9)_{q1} & R(9,9)_{q2} & \cdots & R(9,9)_{q9}\end{bmatrix} \quad (47)$$

is a 9×9 Jacobian matrix containing the partial derivatives of the $\boldsymbol{R}_9$ vector with respect to the generalized coordinates. Incorporating Eq. (45) unaltered into the integration scheme could lead to numerical instability. To avoid this, we employ Baumgarte's scheme [7], where an altered form of Eq. (45), which is known to be numerically stable, is solved. This takes the form:

$$\ddot{z}_c + \alpha\dot{z}_c + \beta z_c = 0 \quad (48)$$

where α and β are chosen via experimentation to ensure numerical stability. Applying Eqs. (44–46) to Eq. (48) and rearranging leads to a form of the constraint equation as incorporated into the numerical integration scheme:

$$\boldsymbol{R}_9^T\cdot\dot{\boldsymbol{p}} = -\{\bar{\boldsymbol{J}}\,\dot{\boldsymbol{q}}\}\cdot\boldsymbol{p} - \alpha\boldsymbol{R}_9^T\cdot\boldsymbol{p} - \beta z_c \quad (49)$$

The first term on the right-hand side contains the Jacobian which is determined numerically in the algorithm. This step is time consuming and slows the integration speed down considerably. For a typical flight disturbed by a 5 m/s gust from the side, Eq. (49) ensures a maximum error in z_c on the order of about 10^{-8} m. Neglecting the first term on the right-hand side of Eq. (49) causes this error peak to grow to about 10^{-5} m, which is still acceptably small. For many simulations it is hence acceptable to perform the calculations without the Jacobian term.

As mentioned before, the analytical dynamics formulation renders the determination of internal loads unnecessary, in general, which is one of its strengths. However, in the case of a parafoil suspended UAV, tension in the suspension lines causes an internal restoring moment at the hinge, directed along the z_p axis, which counteracts relative yaw between the two bodies. The restoring moment acts directly on the ψ_r coordinate and its magnitude is influenced by the suspension line force resultant acting along the z_p axis. To calculate this force, a ninth dummy coordinate, z_c, had to be added to the formulation. Müller [8] derives a mathematical model for the suspension line restoring moment, which is also used in the present method. Closely following this development, it will be assumed that the restoring moment, per unit resultant force, is given by $M_{\text{rest}} = -f_{\text{fudge}}k_{\text{rest}}\sin\sigma$ where k_{rest} depends on the geometry of the configuration and is given by

$$k_{\text{rest}} = \frac{r\sin\psi_r R}{\sqrt{R^2 + r^2 - 2Rr\cos\psi_r}}$$

Generalized Forces

The vector $\boldsymbol{Q}$ on the right-hand side of Eq. (26) represents generalized forces. A generalized force could either be a force or a moment, depending on whether it is associated with a linear or a rotational coordinate. A generalized force Q_i is equal numerically to the virtual work done per unit displacement of its associated

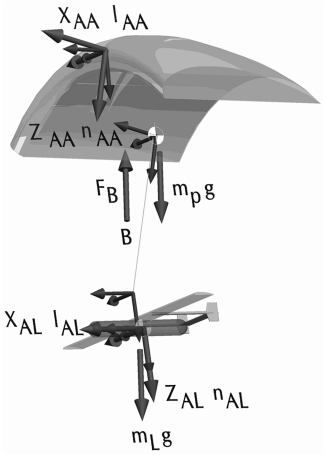

Fig. 2 Forces and moments acting on the configuration.

coordinate q_i, by the forces acting on the system when the other generalized coordinates remain constant. Recalling that weight and buoyancy force are already included in the Lagrangian, $\boldsymbol{Q}$ would be determined by aerodynamic and engine thrust loads, and the internal hinge reaction only. The various forces and moments acting on the configuration are shown in Fig. 2. These loads are now converted to a generalized force for each generalized coordinate.

The resultant force and moment acting at the UAV mass center are obtained first. Taking components in the inertial axes frame, the resultant force acting at L is

$$\boldsymbol{F}^{\,I}_{L} = [T]^T_{LI}\left(\boldsymbol{F}^{L}_{AL} + \boldsymbol{F}^{L}_{tL} + [T]^T_{pL}\boldsymbol{F}^{p}_{AA}\right)$$

where $\boldsymbol{F}^{L,p}_{AL,A} = \{X_{AL,A}\ Y_{AL,A}\ Z_{AL,A}\}^T$ are the aerodynamic force vectors acting on the UAV and the parafoil (including lines and straps), respectively. $\boldsymbol{F}^{L}_{tL}$ is the thrust force, if a propulsive device is active.

The resultant moment at the UAV mass center, in UAV body axes, is

$$\boldsymbol{M}^{\,L}_{L} = \boldsymbol{M}^{L}_{AL} + \boldsymbol{M}^{L}_{tL} + [T]^T_{pL}\boldsymbol{M}^{p}_{AA} + \boldsymbol{r}^{L}_{LA} \times \boldsymbol{F}^{L}_{AA}$$

where $\boldsymbol{M}^{L,p}_{AL,A} = \{\ell_{AL,A}\ m_{AL,A}\ n_{AL,A}\}^T$ are the aerodynamic moment vectors acting on the UAV and the parafoil (including lines and straps), respectively. $\boldsymbol{M}^{L}_{tL}$ is the moment due to thrust. The resultant moment acting at the hinge, due to the aerodynamic loading acting on the parafoil only, in hinge axes, is

$$\boldsymbol{M}^{\,H}_{H} = [T]^T_{pH}\boldsymbol{M}^{p}_{AA} + \boldsymbol{r}^{H}_{HA} \times \boldsymbol{F}^{H}_{AA}$$

The force components are obtained from the aerodynamic coefficients by means of the following relationship:

$$\boldsymbol{F}^{\,L,p}_{AL,A} = \tfrac{1}{2}\rho V^2_{L,Aw} S_{L,p}[T]\,[T]_{L,Aw}\{-C_{DL,A} \quad C_{YL,A} \quad -C_{LL,A}\}^T$$

where, for the UAV and the parafoil, respectively, $[T] = [I]$ and $[T] = [T]_{pA}$. Even in the presence of side slip, the directions of the lift and drag coefficients are often defined such that they lie in the vehicle symmetry plane. Hence one has to set $\beta_{L,A} = 0$ in the transformation matrices $[T]_{L,Aw}$ given in Appendix A. The moment components are given by

$$\boldsymbol{M}^{L}_{AL} = \frac{1}{2}\rho V^2_{Lw} S_L\{\,b_L C_{\ell L} \quad c_L C_{mL} \quad b_L C_{nL}\,\}^T \quad \text{and}$$

$$\boldsymbol{M}^{p}_{AA} = \frac{1}{2}\rho V^2_{Aw} S_p[T]_{pA}\{\tfrac{b_p}{2} C_{\ell A} \quad c_p C_{mA} \quad \tfrac{b_p}{2} C_{nA}\}^T$$

The generalized forces for the X_L, Y_L, and Z_L coordinates are simply the three components of $\boldsymbol{F}^{I}_{L}$. To obtain the generalized forces for the rotational coordinates, the various moments presented above are to be projected onto the respective axes of rotation. The generalized moments for coordinates ψ, θ, and φ are hence given by

$$M_\psi = -M^L_L(1)\sin\theta + M^L_L(2)\cos\theta\sin\phi + M^L_L(3)\cos\theta\cos\phi$$

$$M_\theta = M^L_L(2)\cos\phi - M^L_L(3)\sin\phi \quad \text{and} \quad M_\phi = M^L_L(3)$$

The generalized forces for the two relative rotations are given by

$$M_{\theta r} = M^H_{Hy} \quad \text{and} \quad M_{\psi r} = M^H_{Hz}\cos\theta_r + M^H_{Hx}\sin\theta_r + \lambda M_{\text{rest}}$$

For the z_c coordinate the generalized force is $F_{zc} = -Z_{AA}$. In summary, the generalized force vector is given by

$$\boldsymbol{Q} = \left\{F^I_{Lx} \quad F^I_{Ly} \quad F^I_{Lz} \quad M_\psi \quad M_\theta \quad M_\phi \quad M_{\theta r} \quad M_{\psi r} \quad F_{zc}\right\}^T \tag{50}$$

The parafoil aerodynamic coefficients are obtained by manipulation of results generated by a commercially available CFD code called *PARALABS* [9]. This code, developed specifically for parafoil aerodynamics, is based on a potential flow surface panel method adjusted for separation on the parafoil brakes. The code generates tables of aerodynamic coefficients as functions of angle of attack, relative yaw angle, and brake deflection (one side only). Direct interpolation from the tables is numerically much too slow for flight motion simulations. For this reason functional forms were fitted to the data, enabling rapid computation of coefficients. This computation takes the form:

$$\{C\} = [M]\{P\} \tag{51}$$

where the aerodynamic coefficients are contained in the vector $\{C\}$, as

$$\{C\} = \{C_{D1}\ C_{Y1}\ C_{L1}\ C_{l1}\ C_{m1}\ C_{n1}\ C_{Y\beta}\ C_{l\beta}\ C_{n\beta}\ C_{Dp}\ C_{Yp}\ C_{lp}\ C_{np}\ C_{Dq}\ C_{Lq}\ C_{mq}\ C_{Yr}\ C_{lr}\ C_{nr}\}^T$$

$[M]$ is a matrix, associated with a particular brake setting (one side only), determined by the fitting process,

$$[M] = \begin{bmatrix}
+ & + & + & 0 & 0 & 0 & 0\\
\pm & \pm & \pm & + & + & + & +\\
+ & + & 0 & 0 & 0 & 0 & 0\\
\pm & \pm & \pm & + & + & + & +\\
+ & + & + & 0 & 0 & 0 & 0\\
\pm & \pm & \pm & + & + & + & +\\
+ & + & + & 0 & 0 & 0 & 0\\
+ & + & + & 0 & 0 & 0 & 0\\
+ & + & + & 0 & 0 & 0 & 0\\
+ & 0 & 0 & 0 & 0 & 0 & 0\\
+ & + & + & 0 & 0 & 0 & 0\\
+ & + & + & 0 & 0 & 0 & 0\\
+ & + & + & 0 & 0 & 0 & 0\\
+ & + & + & 0 & 0 & 0 & 0\\
+ & + & + & 0 & 0 & 0 & 0\\
+ & + & + & 0 & 0 & 0 & 0\\
+ & + & + & 0 & 0 & 0 & 0\\
+ & + & + & 0 & 0 & 0 & 0\\
+ & + & + & 0 & 0 & 0 & 0
\end{bmatrix}$$

The plusses and zeros in this matrix indicate nonzero and zero valued coefficients, respectively, and the plus/minuses indicate coefficients experiencing a sign change if the opposite brake is deflected instead. It is easy to show, from symmetry considerations, that the magnitude and sign of derivatives of lateral coefficients such as C_Y, C_ℓ, and C_n with respect to β_A, p_p, and r_p are, respectively, equal for left or right brake equal deflections. $\{P\}$ is a vector representing angle of attack α and relative yaw ψ_r:

$$\{P\} = \{\,1 \quad \alpha_A \quad \alpha_A^2 \quad \psi_r \quad \psi_r^3 \quad \psi_r\alpha_A \quad \psi_r\alpha_A^2\,\}^T$$

For arbitrary brake settings, the vector $\{C_0\}$ is first determined for zero deflection, followed by determining, respectively, for the cases of right and left brake deflections, the vectors $\{C_{\text{right}}\}$ and $\{C_{\text{left}}\}$ via

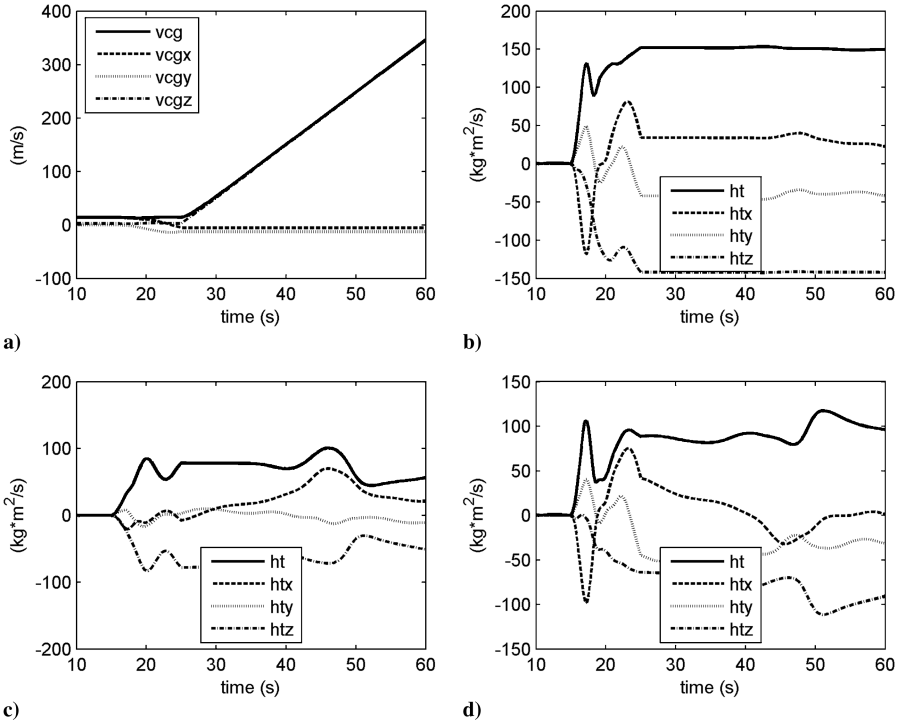

Fig. 3 Simulations with no Jacobian stabilization: a) global mass center inertial velocity; b) global angular momentum; c) UAV angular momentum; and d) parafoil angular momentum.

interpolation. The total effect is obtained as

$$\{C_{\text{tot}}\} = \{C_{\text{right}}\} + \{C_{\text{left}}\} - \{C_0\}$$

Finally, the coefficient vector $\{C_{\text{tot}}\}$ is used to calculate the parafoil aerodynamic coefficients, in parafoil wind axes, as follows:

$$C_{DA} = C_{D1\text{tot}} + C_{Dp}\bar{p}_p + C_{Dq}\bar{q}_p$$
$$C_{YA} = C_{Y1\text{tot}} + C_{Y\beta}\beta_A + C_{Yp}\bar{p}_p + C_{Yr}\bar{r}_p$$
$$C_{LA} = C_{L1\text{tot}} + C_{Lq}\bar{q}_p$$
$$C_{\ell A} = C_{\ell 1\text{tot}} + C_{\ell\beta}\beta_A + C_{\ell p}\bar{p}_p + C_{\ell r}\bar{r}_p$$
$$C_{mA} = C_{m1\text{tot}} + C_{mq}\bar{q}_p$$
$$C_{nA} = C_{n1\text{tot}} + C_{n\beta}\beta_A + C_{np}\bar{p}_p + C_{nr}\bar{r}_p$$

The aerodynamic coefficients for the UAV are calculated in conventional fashion.

Consolidation of Equations

The equations of motion, including the single equation of constraint, can be summarized as follows:

$$[M_d]\{\dot{s}\} = \{y\} \tag{52}$$

where

$$\{\dot{s}\} = \{\, \dot{p}_{XI} \quad \dot{p}_{YI} \quad \dot{p}_{ZI} \quad \dot{p}_{\psi} \quad \dot{p}_{\theta} \quad \dot{p}_{\phi} \quad \dot{p}_{\theta r} \quad \dot{p}_{\psi r} \quad \dot{p}_{z_c} \quad \lambda \,\}^T$$

and

$$\{y\} = \begin{Bmatrix} \boldsymbol{F}_L^I(1) \\ \boldsymbol{F}_L^I(2) \\ \boldsymbol{F}_L^I(3) + m_t g - \rho V g \\ \frac{\partial L}{\partial \psi} + M_{\psi} \\ \frac{\partial L}{\partial \theta} + M_{\theta} \\ \frac{\partial L}{\partial \phi} + M_{\phi} \\ \frac{\partial L}{\partial \theta_r} + M_{\theta r} \\ \frac{\partial L}{\partial \psi_r} + M_{\psi r} \\ \frac{\partial L}{\partial z_c} - Z_{AA} \\ -\{\bar{\boldsymbol{J}}\,\dot{\boldsymbol{q}}\} \cdot \boldsymbol{p} - \alpha \boldsymbol{R}_9^T \cdot \boldsymbol{p} - \beta z_c \end{Bmatrix}$$

At each step during the numerical integration process, $\{\dot{s}\}$ is to be solved from Eq. (52), producing the suspension line force λ in the process. The first nine equations of Eq. (52) hence provide a set of first-order differential equations in the generalized momenta. The other set of nine first-order differential equations that is needed to complete the formulation is given by Eq. (25).

$$[M_d] = \begin{bmatrix} 1 & & & & & & & & & \\ & 1 & & & & & & & & \\ & & 1 & & & & & & & \\ & & & 1 & & & & & & \\ & & & & 1 & & & & & \\ & & & & & 1 & & & & \\ & & & & & & 1 & & & \\ & & & & & & & 1 & & -M_{\text{rest}} \\ & & & & & & & & 1 & 1 \\ R(9,1) & R(9,2) & R(9,3) & R(9,4) & R(9,5) & R(9,6) & R(9,7) & R(9,8) & R(9,9) & 0 \end{bmatrix}$$

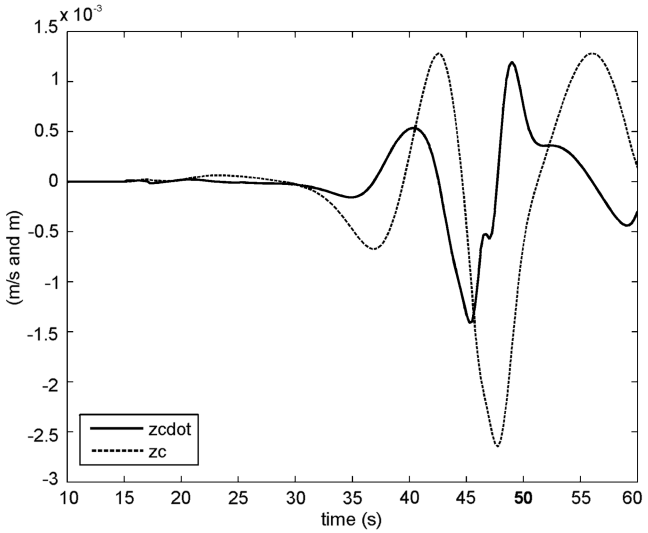

Fig. 4 Satisfaction of $z_c = 0$ constraint with no Jacobian stabilization.

Quality Assurance on Algorithm

The mathematical model described above was programmed for numerical integration in MATLAB. The results reported here were obtained by means of a fixed time step Adams integration procedure. To help ensure that the dynamic model formulation is error free, motion simulations were performed in which, at some instant, the air density was set to zero. Subsequently the trajectory of the system global mass center should describe a parabola in inertial axes, and the angular momentum vector with respect to the global mass center should remain constant.

Figures 3–6 show results for a case in which steady trimmed flight is sustained for 15 s, followed by a 50% left brake application. After another 10 s, the air density is made zero. The asymmetric brake deflection causes three-dimensional flight, posing a thorough test for the dynamics model. For the case where no Jacobian stabilization is incorporated, allowing rapid motion simulation, Fig. 3b shows that global angular momentum is well preserved for about 20 s after vacuum penetration, after which errors develop. As far as the $z_c = 0$ requirement is concerned, Fig. 4 shows that an error of about 3 mm develops toward the end of the simulation.

Figures 5 and 6 represent the case where Jacobian stabilization for the $z_c = 0$ constraint was included. Figure 5b shows much improved conservation of angular momentum for the simulated period of 35 s flight in vacuum. The conservation of global angular momentum is remarkable considering the variations in the individual angular momenta of the two bodies with respect to their own mass centers. It is clear that complex three-dimensional dynamic interaction occurs, but the laws of mechanics are preserved. In the horizontal plane, linear momentum is also conserved as the horizontal global mass center velocity components remain constant. As expected, the vertical velocity component increases linearly with time. The $z_c = 0$ constraint is now better satisfied (Fig. 6), with the maximum error restricted to about 1.5 μm.

Tests for flights in air were performed. For the left turn maneuver discussed above it was found that the $z_c = 0$ constraint with Jacobian stabilization is satisfied to about 10^{-8} m, 2 orders of magnitude better than for the vacuum case. Iosilevskii [10] derived approximate linear solutions for trimmed longitudinal flight, considering the parafoil and payload to be one rigid body. He essentially considered pitching moment balance of the parafoil about the common mass center, leading to, among other things, expressions for trim lift coefficients. Although including the hinge in the present dynamic model results in more complex flight than modeled by Iosilevskii's theory, comparison between the two methods is possible if one sets UAV aerodynamic loads equal to zero and focuses on pitching moment balance about the hinge. Figure 7 compares trim angle-of-attack predictions for various fractions of brake settings. Tests on trim boundaries for longitudinal flight were performed by comparing current results to Iosilevskii's theory. It is known that parafoil trim is strongly influenced by a number of parameters such as positioning of the hinge and aerodynamic coefficients. If, for example, C_{mH} is too large negative for the particular rigging setting, a trim condition does not exist and the configuration would tumble to its doom. Figure 8 shows trim envelopes, defined as limits on the permissible negative C_{mH}, as predicted by means of linear theory. Regions below the parabolas signify instability. Approximate limits of stability as predicted by means of the 8DOF code are superimposed. Agreement is good.

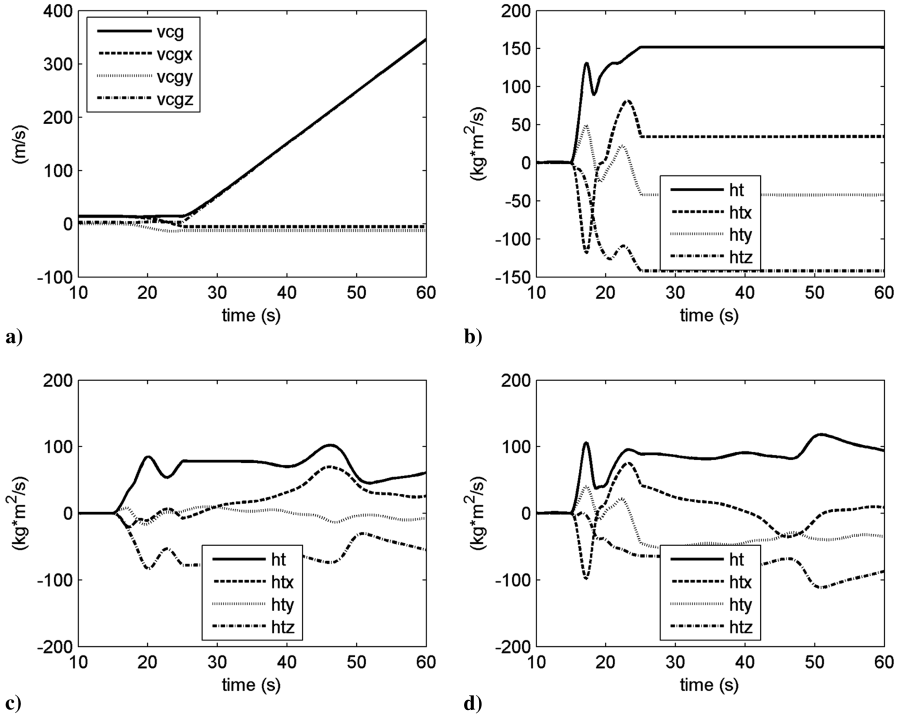

Fig. 5 Simulations with Jacobian stabilization: a) global mass center inertial velocity; b) global angular momentum; c) UAV angular momentum; and d) parafoil angular momentum.

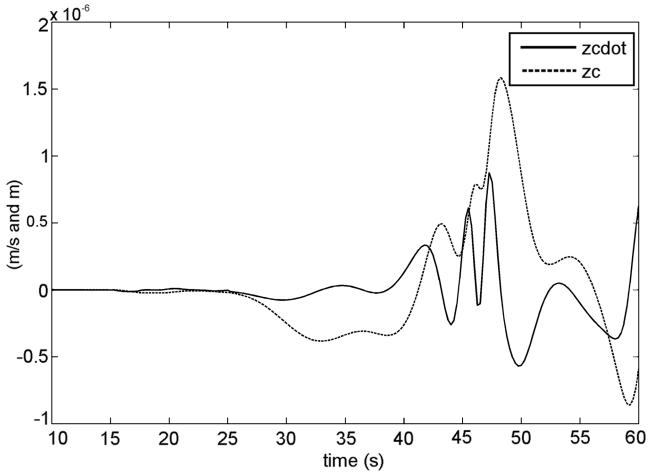

Fig. 6 Satisfaction of the $z_c = 0$ constraint if Jacobian stabilization is applied.

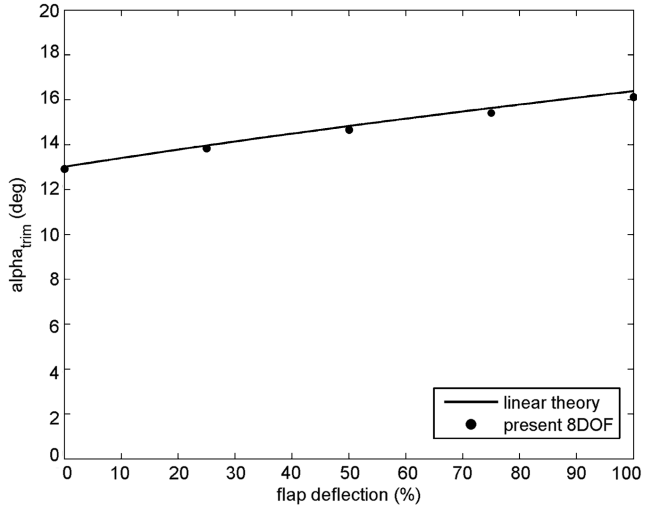

Fig. 7 Trim angle of attack for various brake settings.

In an effort to check three-dimensional flight predictions in the presence of air, 8 degree of freedom (8DOF) flight simulations for a steady turn were compared to moment and force balance requirements for this maneuver. Using a "body" axis system with origin placed at the global mass center, the y axis horizontal and pointing toward the rotation axis, the z axis pointing vertically downward and the x axis completing the right-handed system, it can

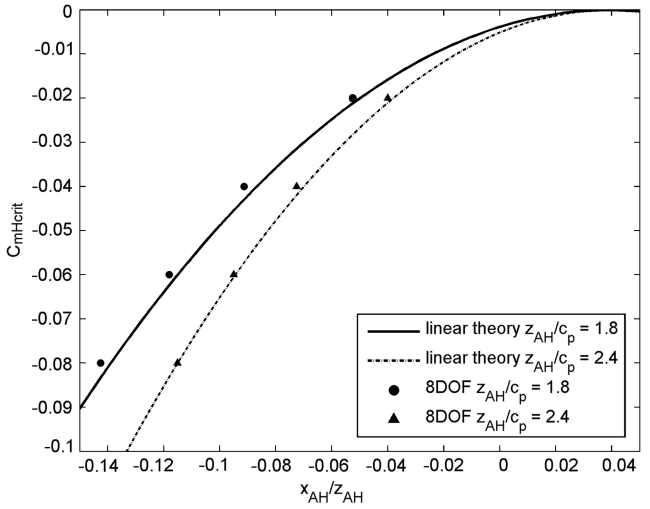

Fig. 8 Critical C_{mH} for stable trim vs hinge position.

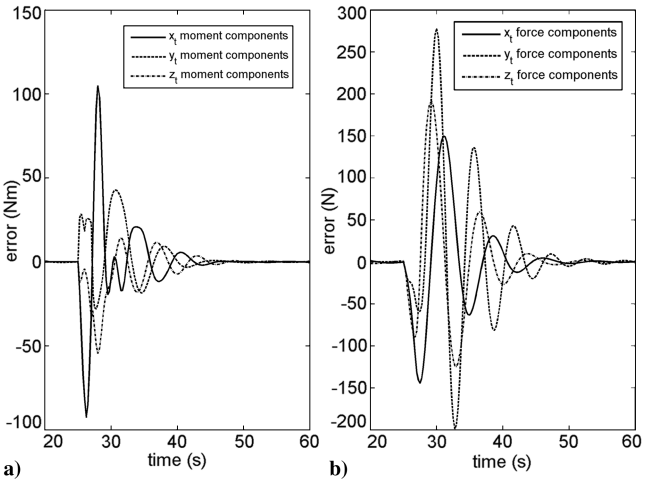

Fig. 9 Results for a turn: a) error in moment balance and b) error in force balance.

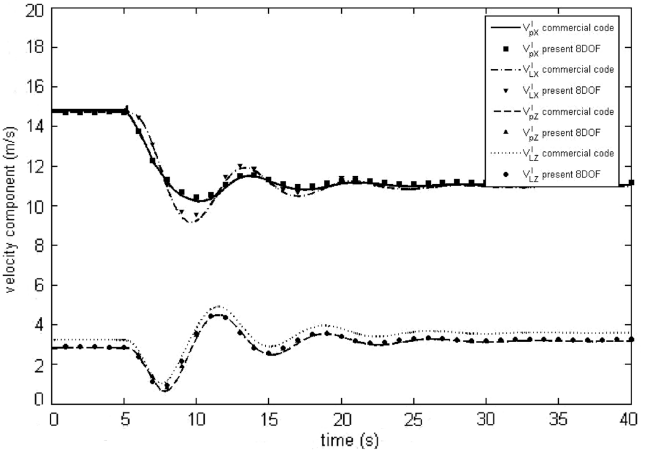

Fig. 10 Comparison of results for a landing flare maneuver.

easily be shown that the conditions for force and moment balance are, respectively,

$$F_{tx} = 0 \qquad F_{ty} = m_t \dot{\psi} V_{c(\text{hor})} \qquad F_{tz} = 0$$

and

$$M_{ctx} = -\dot{\psi}^2 I_{tyz} \qquad M_{cty} = \dot{\psi}^2 I_{txz} \qquad M_{ctz} = 0$$

Simulations were performed for a left turn resulting from a 50% left brake application and the results are shown in Fig. 9. It is clear that force and moment balance requirements are indeed satisfied once transients have died out.

Current results were also compared to those generated by means of a commercially available code [9] for the prediction of parafoil flight. Figure 10 shows results for an important maneuver, the landing flare, achieved by applying a ramped symmetric brake input from zero to 100% over 2 s. Almost identical motions are predicted and a reduction in forward speed and sink rate after brake application is obtained, which is of course a desired response.

Conclusions

A mathematical model, based on an analytic mechanics approach, was developed for the simulation of the flight of a parafoil and air vehicle combination. To the author's knowledge this is the only 8-degree-of-freedom parafoil model based on a Hamiltonian approach that has been developed. A structure for the calculation of parafoil aerodynamic parameters using data from computational fluid dynamics is proposed. The equations as presented here are

programmable with relative ease, avoiding the need to purchase expensive multibody dynamics software. The model was programmed in MATLAB, various simulations were performed, and the results compared with solutions for motion in a vacuum, linearized trim theory and results from another code. Numerical stability of the redundant coordinate and force and moment balance in a steady turn were examined. The current code passed all these tests.

Appendix A: Matrices for Transformation Between Axes Systems

Inertial to UAV body:

$$[T]_{LI} = \begin{bmatrix} \cos\psi\cos\theta & \sin\psi\cos\theta & -\sin\theta \\ -\sin\psi\cos\phi + \cos\psi\sin\theta\sin\phi & \cos\psi\cos\phi + \sin\psi\sin\theta\sin\phi & \cos\theta\sin\phi \\ \sin\psi\sin\phi + \cos\psi\sin\theta\cos\phi & -\cos\psi\sin\phi + \sin\psi\sin\theta\cos\phi & \cos\theta\cos\phi \end{bmatrix} \tag{A1}$$

UAV body to parafoil body:

$$[T]_{pL} = \begin{bmatrix} \cos\theta_r\cos\psi_r & \sin\psi_r & -\sin\theta_r\cos\psi_r \\ -\cos\theta_r\sin\psi_r & \cos\psi_r & \sin\theta_r\sin\psi_r \\ \sin\theta_r & 0 & \cos\theta_r \end{bmatrix}$$

Parafoil aerodynamic to parafoil body:

$$[T]_{pA} = \begin{bmatrix} \cos\theta_A & 0 & -\sin\theta_A \\ 0 & 1 & 0 \\ \sin\theta_A & 0 & \cos\theta_A \end{bmatrix}$$

Wind to parafoil aerodynamic or UAV body:

$$[T]_{L,Aw} = \begin{bmatrix} \cos\beta_{L,A}\cos\alpha_{L,A} & -\sin\beta_{L,A}\cos\alpha_{L,A} & -\sin\alpha_{L,A} \\ \sin\beta_{L,A} & \cos\beta_{L,A} & 0 \\ \cos\beta_{L,A}\sin\alpha_{L,A} & -\sin\beta_{L,A}\sin\alpha_{L,A} & \cos\alpha_{L,A} \end{bmatrix}$$

Appendix B: Various Matrices

Matrix $[V^I_{H/L}]$ Eq. (6):

$$[V^I_{H/L}] = \begin{bmatrix} -\sin\psi\cos\theta\, x_{LH} + (\cos\psi\sin\phi - \sin\psi\sin\theta\cos\phi)z_{LH} & -\cos\psi\sin\theta\, x_{LH} + \cos\psi\cos\theta\cos\phi\, z_{LH} & (\sin\psi\cos\phi - \cos\psi\sin\theta\sin\phi)z_{LH} \\ \cos\psi\cos\theta\, x_{LH} + (\sin\psi\sin\phi + \cos\psi\sin\theta\cos\phi)z_{LH} & -\sin\psi\sin\theta\, x_{LH} + \sin\psi\cos\theta\cos\phi\, z_{LH} & -(\cos\psi\cos\phi + \sin\psi\sin\theta\sin\phi)z_{LH} \\ 0 & -\cos\theta\, x_{LH} - \sin\theta\cos\phi\, z_{LH} & -\cos\theta\sin\phi\, z_{LH} \end{bmatrix}$$

Matrix $[V^p_{p/H}]$ Eq. (8):

$$[V^p_{p/H}] = \begin{bmatrix} -\cos\theta\sin\phi\cos\theta_r z_{pH} & -\cos\phi\cos\theta_r z_{pH} & 0 & -\cos\theta_r z_{pH} & 0 & -\sin\theta_r \\ -(\sin\theta\cos\theta_r + \cos\theta\cos\phi\sin\theta_r)z_{pH} & \sin\phi\sin\theta_r z_{pH} & \cos\theta_r z_{pH} & 0 & 0 & 0 \\ \cos\theta\sin\phi\sin\theta_r z_{pH} & \cos\phi\sin\theta_r z_{pH} & 0 & \sin\theta_r z_{pH} & 0 & -\cos\theta_r \end{bmatrix}$$

Matrix $[H_L]$ Eq. (18):

$$[H_L] = \begin{bmatrix} -I_{Lxx}\sin\theta + I_{Lxz}\cos\theta\cos\phi & -I_{Lxz}\sin\phi & I_{Lxx} \\ I_{Lyy}\cos\theta\sin\phi & I_{Lyy}\cos\phi & 0 \\ I_{Lzz}\cos\theta\cos\phi - I_{Lxz}\sin\theta & -I_{Lzz}\sin\phi & I_{Lxz} \end{bmatrix}$$

Matrix $[H_p]$ Eq. (19):

$$[H_p] = \begin{bmatrix} I_{pxx}\Omega_p(1,1) + I_{pxz}\Omega_p(1,3) & I_{pxx}\Omega_p(2,1) + I_{pxz}\Omega_p(2,3) & I_{pxx}\Omega_p(3,1) + I_{pxz}\Omega_p(3,3) & I_{pxx}\Omega_{pr}(1,1) + I_{pxz}\Omega_{pr}(1,3) & I_{pxx}\Omega_{pr}(2,1) + I_{pxz}\Omega_{pr}(2,3) \\ I_{pyy}\Omega_p(1,2) & I_{pyy}\Omega_p(2,2) & I_{pyy}\Omega_p(3,2) & I_{pyy}\Omega_{pr}(1,2) & I_{pyy}\Omega_{pr}(2,2) \\ I_{pzz}\Omega_p(1,3) + I_{pxz}\Omega_p(1,1) & I_{pzz}\Omega_p(2,3) + I_{pxz}\Omega_p(2,1) & I_{pzz}\Omega_p(3,3) + I_{pxz}\Omega_p(3,1) & I_{pzz}\Omega_{pr}(1,3) + I_{pxz}\Omega_{pr}(1,1) & I_{pzz}\Omega_{pr}(2,3) + I_{pxz}\Omega_{pr}(2,1) \end{bmatrix}$$

Matrix $[\Omega_L]$ Eq. (20):

$$[\Omega_L] = \begin{bmatrix} -\sin\theta & \cos\theta\sin\phi & \cos\theta\cos\phi \\ 0 & \cos\phi & -\sin\phi \\ 1 & 0 & 0 \end{bmatrix}$$

Matrix $[\Omega_{pr}]$ Eq. (22):

$$[\Omega_{pr}] = \begin{bmatrix} \sin\psi_r & \cos\psi_r & 0 \\ 0 & 0 & 1 \end{bmatrix}$$

Matrix $[\Omega_{\Phi L}]$ Eq. (29):

$$[\Omega_{\Phi L}] = \begin{bmatrix} 0 & 0 & 0 \\ -\dot{\psi}\cos\theta & -\dot{\psi}\sin\theta\sin\phi & -\dot{\psi}\sin\theta\cos\phi \\ 0 & -\dot{\theta}\sin\phi + \dot{\psi}\cos\theta\cos\phi & -\dot{\theta}\cos\phi - \dot{\psi}\cos\theta\sin\phi \end{bmatrix}$$

Matrices $[T_{\psi,\theta,\varphi}]_{LI}$ Eq. (32):

$$[T_{\psi}]_{LI} = \begin{bmatrix} -\sin\psi\cos\theta & \cos\psi\cos\theta & 0 \\ -\cos\psi\cos\phi - \sin\psi\sin\theta\sin\phi & -\sin\psi\cos\phi + \cos\psi\sin\theta\sin\phi & 0 \\ \cos\psi\sin\phi - \sin\psi\sin\theta\cos\phi & \sin\psi\sin\phi + \cos\psi\sin\theta\cos\phi & 0 \end{bmatrix}$$

$$[T_{\theta}]_{LI} = \begin{bmatrix} -\cos\psi\sin\theta & -\sin\psi\sin\theta & -\cos\theta \\ \cos\psi\cos\theta\sin\phi & \sin\psi\cos\theta\sin\phi & -\sin\theta\sin\phi \\ \cos\psi\cos\theta\cos\phi & \sin\psi\cos\theta\cos\phi & -\sin\theta\cos\phi \end{bmatrix}$$

$$[T_{\phi}]_{LI} = \begin{bmatrix} 0 & 0 & 0 \\ \sin\psi\sin\phi + \cos\psi\sin\theta\cos\phi & -\cos\psi\sin\phi + \sin\psi\sin\theta\cos\phi & \cos\theta\cos\phi \\ \sin\psi\cos\phi - \cos\psi\sin\theta\sin\phi & -\cos\psi\cos\phi - \sin\psi\sin\theta\sin\phi & -\cos\theta\sin\phi \end{bmatrix}$$

Matrices $[T_{\theta r,\psi r}]_{pL}$ Eq. (41):

$$[T_{\theta r}]_{pL} = \begin{bmatrix} -\sin\theta_r\cos\psi_r & 0 & -\cos\theta_r\cos\psi_r \\ \sin\theta_r\sin\psi_r & 0 & \cos\theta_r\sin\psi_r \\ \cos\theta_r & 0 & -\sin\theta_r \end{bmatrix}$$

$$[T_{\psi r}]_{pL} = \begin{bmatrix} -\cos\theta_r\sin\psi_r & \cos\psi_r & \sin\theta_r\sin\psi_r \\ -\cos\theta_r\cos\psi_r & -\sin\psi_r & \sin\theta_r\cos\psi_r \\ 0 & 0 & 0 \end{bmatrix}$$

Acknowledgment

This work was supported by Denel Aerospace Systems.

References

[1] Wyllie, T., "Parachute Recovery for UAV Systems," *Aircraft Engineering and Aerospace Technology*, Vol. 73, No. 6, 2001, pp. 542–551.

[2] Lingard, J. S., "The Performance and Design of Ram-Air Parachutes," UK Royal Aircraft Establishment, TR-81-103, Farnborough, 1981.

[3] Yakimenko, O. A., "On the Development of a Scalable 8-DOF Model for a Generic Parafoil-Payload Delivery System," AIAA Paper 2005-1665, May 2005.

[4] Pillasch, D. W., and Shen, Y. C., "Parachute/Submunition System Coupled Dynamics," AIAA Paper 1984-0784, April 1984.

[5] Etkin, B., and Reid, L. D., "Dynamics of Flight Stability and Control," 3rd ed., Wiley, New York, 1996, p. 100.

[6] Meirovitch, L., "Methods of Analytical Dynamics," McGraw–Hill, New York, 1988, pp. 91–96.

[7] Haug, E. J., *Computer-Aided Kinematics and Dynamics of Mechanical Systems Vol. 1: Basic Methods*, Allyn and Bacon, Boston, 1989, pp. 257–258.

[8] Müller, S., *Modellierung, Stabilität und Dynamik von Gleitschirmsystemen*, Herbert Utz Verlag, Munich, 2002, pp. 14–18.

[9] Müller, S., Heise, M., and Wagner, O., "PARALABS—An Integrated Design Tool for Parafoil Systems," AIAA Paper 2005-1674, May 2005.

[10] Iosilevskii, G., "Center of Gravity and Minimal Lift Coefficient Limits of a Gliding Parachute," *Journal of Aircraft*, Vol. 32, No. 6, Nov.–Dec. 1995, pp. 1297–1302.